2024 European Control Conference (ECC)
June 25-28, 2024. Stockholm, Sweden

Co-Design of the Control Surface Length and Flutter Control Law of the Mini MUTT Aircraft

Zsombor Wermeser[1], Bela Takarics[1], Bálint Patartics[1] and Bálint Vanek[1]

Abstract— **In current practice, once the initial design of an aircraft is completed, it is often revised based on preliminary control synthesis attempts, creating a back-and-fourth iteration for the refinement of the airframe and the control laws. However, joint optimization of the structure and the controller would be advantageous. In view of this, the present paper proposes a technique for simultaneously tuning the airframe and controller parameters of a flexible aircraft. Specifically, a method is provided for the co-design of the flutter suppression control law and the size of control surfaces of the mini MUTT (Multi Utility Technology Testbed) aircraft. To achieve this, static output feedback is used, and the model of the aircraft is parameterized according to the chord length of the flaps. The flutter suppression problem is articulated as the minimization of a nonlinear cost function that considers the energy in the pitching motion of the aircraft, the control effort, and the weight of the actuators. The assessment of the resulting optimal closed-loop proves that the co-design of structural and control parameters is feasible and converges more efficiently to the global optimum in finite steps than the traditional iterative method.**

I. INTRODUCTION

During a traditional aircraft design process, the airframe is designed first, which is followed by the synthesis of the control system. Hence, the control designers optimize the control laws for the given geometry and structure of the aircraft. This process is often repeated for further refinement; however, the iterations do not guarantee the best possible closed-loop performance. For flexible aircraft, the iteration of control and airframe design is more challenging, as elastic phenomena are more difficult to predict and model than the behavior of rigid aircraft.

Contrary to the iteration, co-design is about finding structural and controller parameters simultaneously, linking control and structural design. Aircraft co-design is a rarely considered topic in the literature. In [1] and [2], baseline control laws are designed using H_∞ synthesis together with control surface (elevon) size and vertical tail surface area, respectively. In both studies, the aircraft are rigid. Co-design for two-dimensional elastic wings with flutter control objective is the subject of [3] and [4]. In [3], the optimal control input is calculated directly, together with the optimal values of several structural parameters. In contrast, the controller is synthesized in [4] using H_∞ synthesis.

In the present paper, a co-design problem is proposed, in which the flutter suppression control law and the control surface length of the mini MUTT aircraft (Multi Utility Technology Testbed) are optimized simultaneously. We demonstrate that this is feasible and that the co-design method yields better performance than the traditional iterative approach. For flutter suppression, static output feedback is applied to the model of the aircraft parameterized by the control surface length. The flutter suppression task is articulated as a disturbance rejection problem, and a nonlinear optimization determines the optimal value of the closed-loop parameters.

Flutter suppression control is an actively researched topic because current aircraft design tends to employ lightweight structures to improve flight efficiency. This aims to reduce fuel consumption, resulting in cost-effective and environmentally friendly operation. To achieve this, the aircraft is equipped with high-aspect-ratio wings [7]. The slender wings reduce induced drag at cruise conditions of the aircraft. The high-aspect-ratio wing surfaces undergo more significant structural deflections at lower airspeeds than low-aspect-ratio wing surfaces. At greater wing flexibility, the inertial and elastic forces become more significant than in the case of rigid wings. The natural frequencies of the aeroelastic modes decrease as the aspect ratio increases. This increase reduces the frequency separation between the aeroelastic and rigid body modes. If the modes are coupled, the undesired flutter phenomena occur. The flutter manifests as unstable oscillations, which may lead to structural failure. For flexible aircraft, the airspeed at which flutter occurs, called the flutter speed, can be low, which can significantly limit the safe airspeed range.

Recently, the use of active control systems to mitigate flutter was investigated in the literature [5], [6], [7]. Such a control system can increase the flutter speed to expand the safe flight envelope. Our goal was to develop an efficient method for the simultaneous synthesis of a flutter suppressor static output feedback and control flap surface length in a co-design framework. The controller obtained in co-design is intended to demonstrate the feasibility of the method, and it does not aim to provide the best possible flutter suppression control performance, such as in [5], [6], [7]. The resulting controller is evaluated in a nonlinear simulation, which proves the validity of the method.

The rest of the paper is divided into three main parts. Section II describes the parametrization, structural-, aeroelastic- and Linear Parameter Varying (LPV) modeling steps of the mini MUTT aircraft. Section III is about the co-design framework. Finally, the optimal closed-loop performance is demonstrated using nonlinear simulations in Section IV.

[1]Zsombor Wermeser, Béla Takarics, Bálint Patartics, Bálint Vanek are with the HUN-REN Insitute for Computer Science and Control in Hungary, H-1111 Budapest, Kende u. 13-17. (emails: wermeser@sztaki.hu, takarics@sztaki.hu, patartics@sztaki.hu, vanek@sztaki.hu)

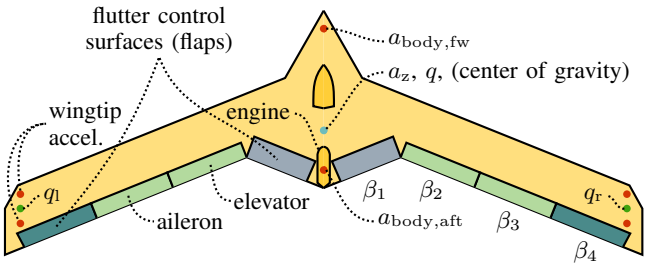

Fig. 1. Sensor and actuator configuration of the mini MUTT aircraft

II. LPV MODELIING OF THE MINI MUTT AIRCRAFT

We use the mini MUTT aircraft for co-design purposes. The mini MUTT is a small, remote-piloted aircraft that resembles Lockheed Martin's Body Freedom Flutter vehicle [8] and NASA's X56 MUTT aircraft [9]. The mini MUTT is developed to demonstrate active aeroservoelastic control technologies [8]. It is a flutter demonstrator since it exhibits body freedom flutter at 25 $\mathrm{m/s}$. The airframe consists of a rigid center body with two flexible wings attached. Each wing is equipped with four control surfaces along the trailing edge, all marked in Fig. 1. Each control flap is utilized for a different purpose. The flaps dedicated to flutter suppression control are indicated in Fig. 1: one pair on the center body and the one closest to the wing tips, with deflection angles denoted by β_1 and β_4, respectively. The control flaps marked with green are the elevators and the ailerons. These control surfaces responsible for the baseline control and the maneuvers, but its do not play a role in the present paper from flutter control aspects.

A. Control Surface Size Parametrization

The parameterization of the control surface length is motivated by the fact that the geometric parameters of the model influence the control laws [1]. The aim is to integrate the control design problem into the aircraft design process; hence, the control surface length parameter is integrated into the model to allow for simultaneous optimization with the control law.

The control surface length parameter, denoted by μ and illustrated in Fig. 2, is the ratio of the chord length of the flap and the nominal chord length. Hence, $\mu = 1$ means the original flap size of the mini MUTT determined by its original designers [10]. Our approach to the parametrization is to construct a set of models of the mini MUTT for discrete values of μ in the interval $[0.75,\ 1.25]$ with resolution $\Delta\mu = 0.0125$. To get a model for any arbitrary μ an interpolation is used between the discretized points after linearization.

The size of the control surface determines the load on the flap, which in turn determines the required actuator mass m_{act} [11]. Different flap sizes require different actuator performance, which results in a larger actuator with a greater performance. Thus, the actuator masses are the function of μ. In the present paper, the numerical values taken from [11] are scaled up by 150% for safety reasons. The actuators are placed on the flexural axis of the wing, similarly to [6], [11]. However, the weight increase makes the bending inertia of the wing more significant; therefore, the inertia is also the function of μ. The variation of the wing structural properties with μ affects the critical flutter speed, as depicted in Fig. 3.

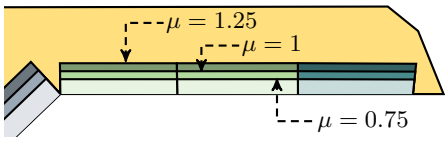

Fig. 2. Parametrized control surface length for the mini MUTT

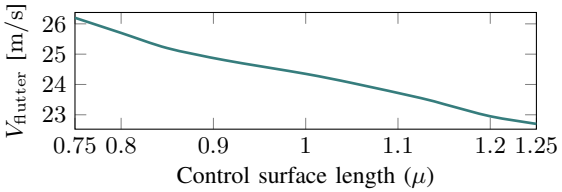

Fig. 3. Flutter speed at different control surface lengths

B. Aeroelastic Aircraft Modeling

The aeroelastic model of the aircraft is composed of three components: aerodynamics, structural dynamics, and rigid dynamics, as illustrated in Fig. 4. These components are elaborated in Sections II-C–D. The Aeroservoelastic Group of the University of Minnesota developed the aerodynamics design of the aircraft, created the `DLMTools` for the aerodynamic and control design, and implemented the nonlinear model in Simulink. All data and information can be downloaded from their website [10].

The original nonlinear model in [10] and used in [6] is augmented by adding wind disturbance inputs along the axes of the North-East-Down coordinate frame. The wind and atmospheric disturbances affect the airspeed, angle of attack, and side-slip angle. These quantities determine the aerodynamic forces and moments acting on the vehicle, thereby influencing the equations of motion of the UAV. The awaking forces and moments are written in detail in [12].

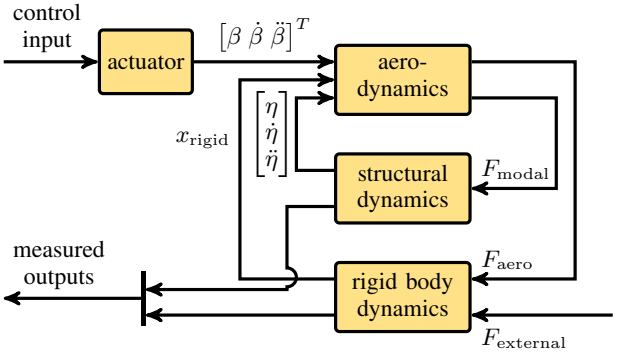

Fig. 4. Interconnection of the components of the aeroelastic aircraft model

Fig. 5. Nodes in the finite element model of the Mini MUTT [14]

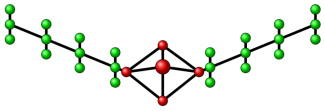

Fig. 6. Spline grid of the mini MUTT [14]

C. Rigid Body and Structural Dynamics

The rigid dynamics component in Fig. 4, is described by the equations of motion [13],

$$\begin{bmatrix} mI & 0 \\ 0 & J_{\text{rig}} \end{bmatrix} \begin{bmatrix} \dot{V}_{\text{r}} \\ \dot{\Omega}_{\text{r}} \end{bmatrix} + \begin{bmatrix} mI\Omega_{\text{r}} \times V_{\text{r}} \\ \Omega_{\text{r}} \times J_{\text{rig}}\Omega_{\text{r}} \end{bmatrix} = \begin{bmatrix} \sum F_{\text{i}} \\ \sum M_{\text{i}} \end{bmatrix}, \quad (1)$$

where m and J_{rig} are the mass and rigid inertia of the aircraft, Ω_{r} and V_{r} are the angular and translational velocities with respect to the inertial axes. F_{i} and M_{i} denote the forces and moments along the mean axes.

The structural dynamics model employs the finite element method. Euler-Bernoulli beams with additional torsional components and point masses are used to build up the model in Fig. 5. The nodes at which the beams are connected have 3 degrees of freedom, namely heaving, bending, and twisting. The structural model is described in modal coordinates as

$$M\ddot{\eta} + C\dot{\eta} + K\eta = F_{\text{modal}}, \quad (2)$$

where M, C, K are the modal mass, damping and stiffness matrices, η is the modal coordinate and F_{modal} is the external excitation expressed in modal coordinates. Due to the parametrization of the control flap size, each aircraft version is obtained by scaling the actuator masses. The matrices M and K depend on μ because the actuator masses are the functions μ.

D. Unsteady Aerodynamic Model

During flight, the flexible airframe deforms, which causes varying flow characteristics. Aeroelastic modeling mainly focuses on capturing the interaction of the deforming airframe and the time-varying flow. Unsteady aerodynamic modeling is required to accurately predict the dependency of aerodynamic forces and moments on the frequency of the dynamic motions. *Vortex-Lattice Method* (VLM) determines the static load case at zero oscillating frequency. VLM is extended by the *Doublet-Lattice Method* (DLM), which provides the aerodynamic force distribution for a given normalwash distribution on the aerodynamic grid at a particular oscillating frequency. The aerodynamic grid should interact with the structural grid to produce coupled aerodynamic phenomena, such as flutter. An additional spline grid is constructed to project the modal displacements on the aerodynamic grid. The spline grid of the mini MUTT is presented in Fig. 6.

The DLMTools toolbox in MATLAB generates the *Aerodynamic Influence Coefficient* (AIC) matrix for the given aerodynamic grid, from which the *Generalized Aerodynamic Matrix* (GAM) is obtained [11], [14]. GAM is the unsteady aerodynamic model expressed in structural modal coordinates, which maps modal deformations to the aerodynamic force distribution in the frequency domain. To get a continuous model in the time domain, Roger's rational function approximation (RFA) is used [14], [15]. Additional lag states are introduced to represent the lag behavior of the aerodynamic model. The states-space dynamics of the lag states are of the form [11]

$$\begin{aligned} \dot{x}_{\text{lag}} &= \frac{2V}{\bar{c}} A_{\text{lag}} x_{\text{lag}} + B_{\text{lag}} [\dot{x}_{\text{rigid}} \ \dot{\mu} \ \dot{\beta}]^{\text{T}}, \\ y_{\text{lag}} &= C_{\text{lag}} x_{\text{lag}}. \end{aligned} \quad (3)$$

Combining the structural dynamics data coming from the FEM model, the unsteady aerodynamics data from DLM-Tools, the missing aerodynamic coefficients from the XFLR-5 software generated by [11] and applying the mean axis approach, the nonlinear parametric aeroelastic model of the mini MUTT aircraft is constructed.

E. Model Reduction

The nonlinear model of the mini MUTT consists of 82 states, from which 46 are aerodynamic lagstates, 16 are structural dynamics states, 12 are rigid body, and 4×2 are actuator dynamics states. Futaba S9254 servos actuate the flutter suppression surfaces on the Mini MUTT [11]. To obtain a numerically tractable model for control design, the components of the aeroservoelastic model in Fig. 4 are reduced by the so-called 'bottom-up' technique in [15]. In essence, the components of the model (i.e., the aero-, structural, and rigid body dynamics) are reduced separately and then combined to obtain the simplified model. Two principles guide the state order reduction of the model components. Firstly, the body freedom flutter is tied to the symmetric deformations of the airframe; therefore, only the symmetric modes of the model are kept. Secondly, the frequency range in which the reduced model is expected to match the high-order model is limited to $[0, \ 100 \ \text{rad/s}]$. This corresponds to the $133 \ \text{rad/s}$ bandwidth of the actuator as it is well above the $30 \ \text{rad/s}$ flutter frequency. Based on these, the first four modes of the structural dynamics, the corresponding four lag states, and θ, q, u, and w in the rigid body dynamics are retained. Together with the actuator states, the reduced model contains 18 states.

F. LPV Model of the Aircraft

The reduced model of the mini MUTT aircraft described thus far in Section II-E is nonlinear. For control design, it is linearized for a set of trim conditions: straight and level flight at 26 equidistant points of the airspeed in $[20, \ 45] \ \text{m/s}$ and 40 equidistant points of μ in $[0.75, \ 1.25]$. In MATLAB-Simulink, `findop` is used to find the trimpoints. The trimmed elevator deflection angle, as in the function of control surface length, is illustrated in Fig. 7. The trim values are continuous and vary according to the required pitching moment for each control surface length. The linear models

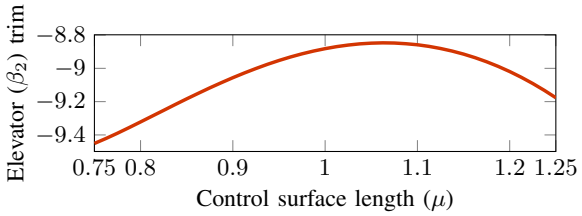

Fig. 7. Trimmed elevator angles to the corresponding control surface lengths

TABLE I
CONTROL CASES

OL	open-loop
1DoF	one degree of freedom, $\beta = \beta_1 = \beta_4$
2DoF	two degrees of freedom, using β_1 and β_4 independently

are obtained from the `linearize` function, and then each resulting Linear Time-Invariant (LTI) model is on the μ - V_{air} grid. From the set of reduced linear models, we construct a Linear Parameter-Varying (LPV) system of the form

$$\begin{aligned} \dot{x} &= A(\rho)x + B(\rho)u, \\ y &= C(\rho)x + D(\rho)u, \end{aligned} \tag{4}$$

where the scheduling parameter $\rho = \begin{bmatrix} V_{\text{air}} & \mu \end{bmatrix}^T$. For arbitrary values of the V_{air} and μ in the given intervals, the state-space matrices are obtained by spline interpolation. This is chosen instead of a second-order and the usual linear interpolation because it provides the required accuracy when comparing the interpolated state-space matrices to the linearized model between grid points.

III. CO-DESIGN PROBLEM FORMULATION

A. Flutter Control Law Parametrization

The flutter controller is chosen as a static output feedback gain for ease of parameterization. The LPV model has six outputs. These are the vertical accelerations at the center of gravity (a_{z}) and two points fore and aft at the body ($a_{\text{body,fw}}$, $a_{\text{body,aft}}$), depicted in Fig. 1. Pitch rate is also measured at the center of gravity q, and at the left q_{l} and right q_{r} wingtips. These measurements are combined into two signals. One of them is the relative angular rate of the wing in the torsional direction, which is defined as $y_{\text{q}} := q_{\text{l}} + q_{\text{r}} - 2 \cdot q_{\text{z}}$. The other one is the relative pitching acceleration of the body, which is $y_{\text{a}} := a_{\text{body,aft}} + a_{\text{body,fw}} - 2 \cdot a_{\text{z}}$. The mini MUTT exhibits body freedom flutter, manifesting as pitching oscillation. These two signals are used for the flutter suppression.

The reduced LPV model in Section II-F has four control inputs, that are the four flutter control flap deflections in Fig. 1, denoted by β_1 and β_4. We define two separate control scenarios in Table I. In the 1DoF case, all flaps are deflected identically, i.e., the control input is a single $\beta := \beta_1 = \beta_4$. The inner and outer flaps are used independently in the 2DoF case. The flutter suppression control laws are of the form 5-6,

$$\text{1DoF:} \qquad \beta(t) = K_1 \cdot y_{\text{a}} + K_2 \cdot y_{\text{q}}, \tag{5}$$

$$\text{2DoF:} \qquad \begin{cases} \beta_1(t) = K_1 \cdot y_{\text{a}} + K_2 \cdot y_{\text{q}}, \\ \beta_4(t) = K_3 \cdot y_{\text{a}} + K_4 \cdot y_{\text{q}}. \end{cases} \tag{6}$$

TABLE II
OUTPUT SIGNAL COMBINATIONS

Gain	Signal Combination ($y(t)$)	Notation
K_1 (K_3)	$a_{\text{body,aft}} + a_{\text{body,fw}} - 2 \cdot a_{\text{z}}$	y_{a}
K_2 (K_4)	$q_{\text{l}} + q_{\text{r}} - 2 \cdot q_{\text{z}}$	y_{q}

where K_1, K_2, K_3, K_4 are output feedback gains to be tuned.

B. Optimal Flutter Control Problem Formulation

The flutter suppression control problem is articulated as an optimal disturbance rejection task. The cost function takes into account the energy in the pitching motion of the center body, the energy in the torsional movement of the wing, the control effort, and the mass of the actuators. It has the form,

$$J(\mu, K) = \int_0^T \left(w_{\text{a}} y_{\text{a}}^2 + w_{\text{q}} y_{\text{q}}^2 + w_\beta \beta^2 \right) \mathrm{d}t + \frac{w_{\text{m}}}{2} m_{\text{act}}, \tag{7}$$

where m_{act} is the mass of all the actuators on the wing (see SectionII-A), and the weighting terms are $w_{\text{a}} = 10^{-2}$, $w_\beta = 100$, $w_{\text{m}} = 10^{-3}$ and $w_{\text{q}} = 1$. The weights are chosen such that the terms have the same order of magnitude. When the 2DoF control case is used, replace the $w_\beta \beta^2$ term with $\frac{w_\beta}{2}\beta_1^2 + \frac{w_\beta}{2}\beta_4^2$.

The objective function in (7) is evaluated for time domain simulations of the linear model. These simulations are conducted at straight and level flight at $V_{\text{air}} = 27$ m/s, which is above the flutter speed for all values of μ. The simulation is run for both *1-cosine* and turbulent wind disturbances for 5 sec time intervals. The used disturbances are presented in Fig. 8. The wind gust velocity varies randomly in the turbulence case, whereas in the *1-cosine* case, it varies deterministically [16]. The gusts are in the vertical direction, assumed constant across the aircraft span [17]. The final value of the objective function evaluated according to (7) for the two wind disturbances, then summed up as $J = J_{\text{turb}} + J_{\text{cos}}$, where J_{turb} and J_{cos} have comparable values.

C. Finding the Optimum of the Cost Function

We find the optimum of the cost function using the `fmincon` function in MATLAB, with the *Sequential Quadratic Programmig* (SQP) algorithm and central differencing scheme to find the optimal direction during the iterations. The upper and lower bounds and the initial values of the decision variables are found in Table III. The feedback gains are not constrained to allow for finding the optimal amplification gain for the error functions. As indicated in Table IV, the variables are initialized with the open loop setup, i.e., zero gains and $\mu = 1$. The optimization employs MATLAB's built-in `GlobalSearch` method to avoid local minima. The optimization is performed on both the LTI model corresponding to $V_{\text{air}} = 27$ m/s and both on the LPV model of the mini MUTT in Section II-F. The simulation of the LPV model is conducted using the `LPVTools` open-source package [18].

TABLE III

UPPER AND LOWER BOUNDS OF THE DESIGN VARIABLES

Design variable	Lower Bound	Upper Bound	Initial Cond.
μ	0.75	1.25	1
K_1 (K_3)	$-\infty$	∞	0
K_2 (K_4)	$-\infty$	∞	0

TABLE IV

SETUP COMBINATIONS FOR CO-DESIGN

Case	μ	Control Law
A	μ_{free}	1DoF
B	fixed to $\mu = 1$	1DoF
C	μ_{free}	2DoF
D	fixed to $\mu = 1$	2DoF

During the simulation, if the airspeed varies on a wide range around 27 $\mathrm{m/s}$, then the LPV model in the optimization is more accurate than the LTI. At the beginning of the iterative optimization process, the airspeed varies on a larger scale; hence, employing the LPV model is advantageous. However, close to the optimum, the speed of the closed-loop deviates very little from 27 $\mathrm{m/s}$, which situation is described accurately by the LTI model. We obtained the same optimum using both the LTI and LPV models; therefore, the LTI model is sufficient for our simulation scenario. Using the LPV could lead to improved results for more complicated maneuvers; however, at the cost of a significant increase in computational complexity. The optimization in the 1DoF case with the LTI model takes approximately 15 minutes on a regular PC. The 2DoF case doubles this computation time to about 30 min. When the LPV model is used, finding a single local optimum with `GlobalSearch` takes about 30 min.

IV. EVALUATION OF THE OPTIMAL CLOSED-LOOP PERFORMANCE

A. Optimal Values Found

We conduct the optimization for four cases summarised in Table IV. In Cases A and C, the design variables (μ, K_1, K_2, K_3, and K_4) are optimized jointly. In Cases B and D, the controllers are optimized for the nominal structure of the mini MUTT. The optimal values for the design variables found by nonlinear optimization are listed in Table V. The 2DoF control law, see in Table I, provides a lower cost than 1DoF. This is reasonable because the controller has more degrees of freedom to interact with the airflow to mitigate flutter. However, the computational time is increased for 2DoF. We note that choosing a higher w_β results in smaller β values with higher μ.

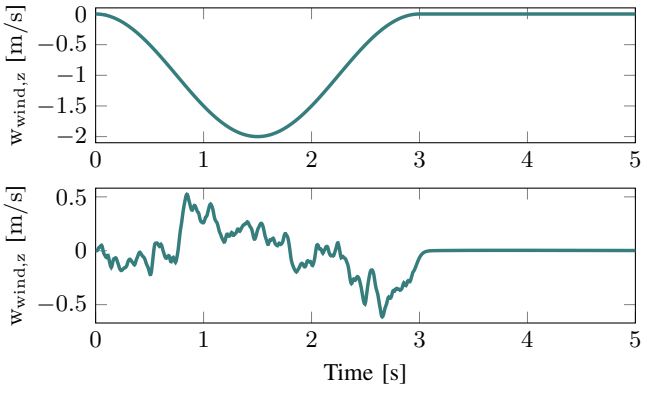

Fig. 8. The two wind disturbances used in evaluation of the objective function J.

TABLE V

OPTIMAL DESIGN VARIABLES FOR THE GIVEN SETUPS

Case	A	B	C	D
μ	0.9187	1	1.0934	1
K_1	-0.7727	-0.8738	-0.3377	-0.2803
K_2	-0.0585	-0.0584	-0.0980	-0.1033
K_3	-	-	-0.7353	-0.5326
K_4	-	-	-0.0636	-0.0434
J	0.4655	0.472	0.3009	0.3103

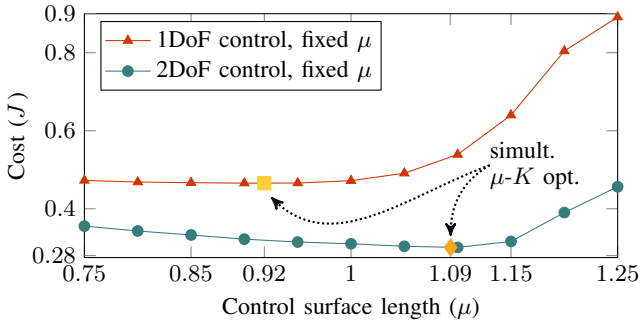

Fig. 9. Comparison of the sequential optimization results and the simultaneous optimum

Cases B and D represent a sequential design approach. The cost values indicate that the sequential method provides less efficient overall performance than the simultaneously optimized controller. To prove that our method can find the global optimum, the optimization in Section III-B is performed for several fixed μ values. The resulting optimal cost function values as a function of the fixed μ are depicted in Fig. 9. The graphs show the achievable optimum if we consider the airframe given and tune the control laws only. These results demonstrate that the co-design method finds the global optimum, which the sequential method cannot reach as efficiently.

B. Simulation of the Optimal Closed Loop

The performance of the optimal closed-loop system is demonstrated using the nonlinear model of the mini MUTT. We conduct the same simulation circumstances used in the optimization but with the nonlinear model of the mini MUTT. Control flap deflections during the simulation are depicted in Fig. 10. According to the figure, small deflections can suppress the flutter. The performance of the controller is evaluated using the relative acceleration of the wingtips (see Fig. 1), defined as the difference between the sum of the local accelerations and the acceleration of the center of gravity. These are depicted in Fig. 11. Even though the

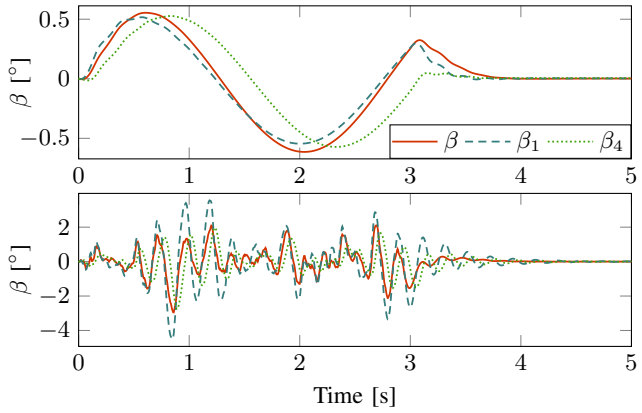

Fig. 10. Control surface angles

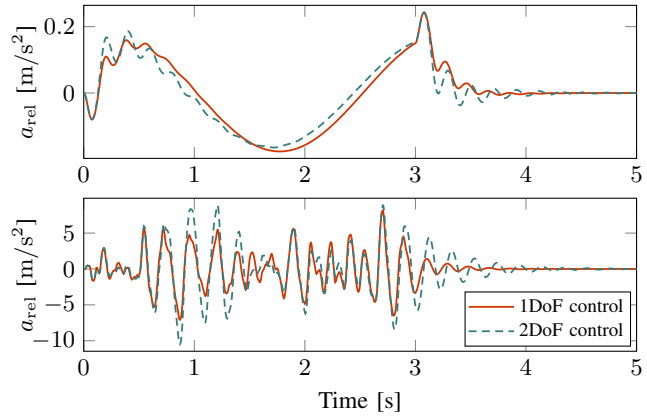

Fig. 11. Acceleration of wing tips relative to the body during the nonlinear simulation

aircraft flies above the open-loop flutter speed, the relative accelerations are low, indicating moderate aerodynamic loads on the wings. The aircraft maintains its stability. These results show that the co-design results in a controller that also suppresses flutter for the nonlinear model, thus proving the applicability of our approach.

V. CONCLUSIONS

This paper presents the co-design of the control surface length and flutter control gains of the flexible mini MUTT aircraft. A model of the aircraft is used, which is parameterized according to the chord length of the flaps, and a static output feedback controller is applied for flutter suppression. A simulation-based nonlinear optimization is performed to find the simultaneous optimum of the variables. This approach leads to stable closed-loops with limited control effort ($|\beta| < 5°$) in reasonable computation times (about 30 minutes), which proves the applicability of the co-design concept. It is further shown that the optimal values for the nominal control surface length, which are 91.87% for the 1DoF scenario and 109.38% for the 2DoF scenario, represent the global optimum. Nonlinear simulations demonstrate the stability and performance of the optimal closed-loops. Future work includes the articulation of the task as an H_∞ control problem and using structured H_∞ synthesis to find the simultaneous optimum.

ACKNOWLEDGMENT

The research leading to these results is part of the FLIPASED projects. This project has received funding from the Horizon 2020 research and innovation programme of the European Union under grant agreement No. 815058. Our research was also supported by the European Union within the framework of the National Laboratory for Autonomous Systems (RRF-2.3.1-21-2022-00002).

REFERENCES

[1] Y. Denieul, J. Bordeneuve-Guibé, D. Alazard, C. Toussaint, and G. Taquin, "Integrated design of flight control surfaces and laws for new aircraft configurations," *IFAC-PapersOnLine*, vol. 50, pp. 14180–14187, July 2017.

[2] E. N. Van, D. Alazard, C. Döll, and P. Pastor, "Co-design of aircraft vertical tail and control laws using distributed electric propulsion," *IFAC-PapersOnLine*, vol. 52, no. 12, pp. 514–519, 2019.

[3] G. Filippi and J. Morlier, "Integrated structural and control system design for robust flutter performance," *ISAE-SUPAERO Institut Suprieur de l'Aronautique et de l'Espace*, p. 6, 2018.

[4] E. Faïsse, R. Vernay, F. Vetrano, D. Alazard, and J. Morlier, "Adding Control in Multidisciplinary Design Optimization of a Wing for Active Flutter Suppression," in *AIAA Scitech 2021 Forum*, (Virtual event), American Institute of Aeronautics and Astronautics, Jan. 2021.

[5] E. Livne, "Aircraft Active Flutter Suppression: State of the Art and Technology Maturation Needs," *Journal of Aircraft*, vol. 55, pp. 410–452, Jan. 2018.

[6] J. Theis, H. Pfifer, and P. J. Seiler, "Robust Control Design for Active Flutter Suppression," in *AIAA Atmospheric Flight Mechanics Conference*, (San Diego, California, USA), American Institute of Aeronautics and Astronautics, Jan. 2016.

[7] B. Patartics, G. Liptak, T. Luspay, P. Seiler, B. Takarics, and B. Vanek, "Application of Structured Robust Synthesis for Flexible Aircraft Flutter Suppression," *IEEE Trans. Contr. Syst. Technol.*, vol. 30, pp. 311–325, Jan. 2022.

[8] J. Beranek, L. Nicolai, M. Buonanno, E. Burnett, C. Atkinson, B. Holm-Hansen, and P. Flick, "Conceptual Design of a Multi-Utility Aeroelastic Demonstrator," in *13th AIAA/ISSMO Multidisciplinary Analysis Optimization Conference*, (Fort Worth, Texas), American Institute of Aeronautics and Astronautics, Sept. 2010.

[9] J. J. Ryan and J. T. Bosworth, "Current and Future Research in Active Control of Lightweight, Flexible Structures Using the X-56 Aircraft," in *52nd Aerospace Sciences Meeting*, (National Harbor, Maryland), American Institute of Aeronautics and Astronautics, Jan. 2014.

[10] Aeroservoelastic-Group-UMN. `https://dept.aem.umn.edu/~AeroServoElastic/research.shtml`. Accessed on 2023-10.

[11] R. D. Mocsányi, B. Takarics, A. Kotikalpudi, and B. Vanek, "Grid-Based and Polytopic Linear Parameter-Varying Modeling of Aeroelastic Aircraft with Parametric Control Surface Design," *Fluids*, vol. 5, p. 47, Apr. 2020.

[12] R. W. Beard and T. W. McLain, *Small unmanned aircraft: theory and practice*. Princeton, N.J: Princeton University Press, 2012. OCLC: ocn724663112.

[13] D. K. Schmidt, *Modern flight dynamics*. New York, NY: McGraw-Hill, 2012.

[14] A. Kotikalpudi, *Robust Flutter Analysis for Aeroservoelastic Systems*. PhD thesis, University of Minnesota, 2017.

[15] B. Takarics, B. Vanek, A. Kotikalpudi, and P. Seiler, "Flight control oriented bottom-up nonlinear modeling of aeroelastic vehicles," in *2018 IEEE Aerospace Conference*, (Big Sky, MT), pp. 1–10, IEEE, Mar. 2018.

[16] H. I. Flomenhoft, "Brief history of gust models for aircraft design," *Journal of Aircraft*, vol. 31, pp. 1225–1227, Sept. 1994.

[17] J. Wright and J. Cooper, *Introduction to Aircraft Aeroelasticity and Loads*. Aerospace Series, Wiley, 2008.

[18] A. Hjartarson, P. Seiler, and A. Packard, "LPVTools: A Toolbox for Modeling, Analysis, and Synthesis of Parameter Varying Control Systems**This work was supported by a NASA Small Business Innovation Research contract from NASA Armstrong Flight Research Center. Contract Monitor is Dr. Martin J. Bren-ner.," *IFAC-PapersOnLine*, vol. 48, no. 26, pp. 139–145, 2015.